Changes in mean-squared charge radii and magnetic moments of $^{179-184}$Tl measured by in-source laser spectroscopy

A. E. Barzakh,[1,*] A. N. Andreyev,[2,3] T. E. Cocolios,[4,5] R. P. de Groote,[4] D. V. Fedorov,[1] V. N. Fedosseev,[6] R. Ferrer,[4] D. A. Fink,[6,7] L. Ghys,[4,8] M. Huyse,[4] U. Köster,[9] J. Lane,[10] V. Liberati,[10] K. M. Lynch,[5,6,11] B. A. Marsh,[6] P. L. Molkanov,[1] T. J. Procter,[6,11] E. Rapisarda,[4,5] S. Rothe,[6,12] K. Sandhu,[10] M. D. Seliverstov,[1] A. M. Sjödin,[6] C. Van Beveren,[4] P. Van Duppen,[4] M. Venhart,[13] and M. Veselský[13]

[1]*Petersburg Nuclear Physics Institute, NRC Kurchatov Institute, 188300 Gatchina, Russia*
[2]*Department of Physics, University of York, YO10 5DD, United Kingdom*
[3]*Advanced Science Research Center (ASRC), Japan Atomic Energy Agency (JAEA), Tokai-mura, Ibaraki 319-1195, Japan*
[4]*KU Leuven, Instituut voor Kern- en Stralingsfysica, B-3001 Leuven, Belgium*
[5]*ISOLDE, CERN, CH-1211 Geneve 23, Switzerland*
[6]*Engineering Department, CERN, CH-1211 Geneve 23, Switzerland*
[7]*Ruprecht-Karls Universität, D-69117 Heidelberg, Germany*
[8]*Belgian Nuclear Research Centre SCK•CEN, Boeretang 200, B-2400 Mol, Belgium*
[9]*Institut Laue Langevin, 6 rue Jules Horowitz, F-38042 Grenoble Cedex 9, France*
[10]*School of Engineering and Science, University of the West of Scotland, Paisley PA1 2BE, United Kingdom*
[11]*School of Physics and Astronomy, The University of Manchester, Manchester M13 9PL, United Kingdom*
[12]*Institut für Physik, Johannes Gutenberg-Universität Mainz, D-55128 Mainz, Germany*
[13]*Institute of Physics, Slovak Academy of Sciences, 845 11 Bratislava, Slovakia*

(Received 25 September 2016; revised manuscript received 13 November 2016; published 23 January 2017)

Hyperfine structure and isotope shifts have been measured for the ground and isomeric states in the neutron-deficient isotopes $^{179-184}$Tl using the 276.9-nm transition. The experiment has been performed at the CERN-Isotope Separator On-Line facility using the in-source resonance-ionization laser spectroscopy technique. Spins for the ground states in ^{179,181,183}Tl have been determined as $I = 1/2$. Magnetic moments and changes in the nuclear mean-square charge radii have been deduced. By applying the additivity relation for magnetic moments of the odd-odd Tl nuclei the leading configuration assignments were confirmed. A deviation of magnetic moments for isomeric states in ^{182,184}Tl from the trend of the heavier Tl nuclei is observed. The charge radii of the ground states of the isotopes $^{179-184}$Tl follow the trend for isotonic (spherical) lead nuclei. The noticeable difference in charge radii for ground and isomeric states of ^{183,184}Tl has been observed, suggesting a larger deformation for the intruder-based $9/2^-$ and 10^- states compared to the ground states. An unexpected growth of the isomer shift for ^{183}Tl has been found.

DOI: 10.1103/PhysRevC.95.014324

I. INTRODUCTION

The region of the neutron-deficient isotopes near the proton shell closure at $Z = 82$ has drawn considerable interest as it exhibits a clear manifestation of shape coexistence in nuclei ([1,2]; recent work has been summarized in Ref. [3]). Isotope shift (IS) or isomer-shift and hyperfine splitting data obtained by laser spectroscopy are of primary importance in these studies. Along with shape coexistence, a pronounced shape staggering was observed in this region of the nuclide chart for the neutron-deficient mercury (Hg) isotopes. Optical and laser spectroscopy measurements [4] have shown that the ground states of the odd-A ^{181,183,185}Hg isotopes ($N = 101,103,105$) are strongly deformed, probably of the prolate type, whereas the even-A isotopes remain weakly deformed, probably of the oblate type, at least down to ^{182}Hg. The weakly oblate character of the ground states of the even $^{182-188}$Hg has been determined through Coulomb excitation measurements [5]. At the same time, the nearby odd-A and even-A lead (Pb) isotones remain nearly spherical down to ^{181}Pb ($N = 99$) [6].

The thallium (Tl) ($Z = 81$) isotope chain is intermediate between the Pb ($Z = 82$) and the Hg ($Z = 80$) chains, therefore it is important to extend the Tl systematics of IS and hyperfine structure (hfs) measurements far in the neutron-deficient region where the Hg systematics differ greatly from those of Pb. So far IS and hfs measurements are limited for the ground states down to ^{183}Tl and for the isomeric states down to ^{185}Tl [7,8]. In the spherical shell-model approach, the spin parity of $I^\pi = 1/2^+$ for the ground states of all presently known odd-A Tl isotopes can be understood as being due to the "normal" $\pi 3s_{1/2}$ proton-hole orbital. The so-called proton "intruder" excited states with $I^\pi = 9/2^-$, involving one-particle two-hole $\pi(1p-2h)$ excitations to the $\pi 1h_{9/2}$ orbital above the $Z = 82$ shell closure, are also well known down to ^{181}Tl [3]. Alternatively, within the deformed mean-field approach, the $I^\pi = 9/2^-$ states can be interpreted as being oblate deformed,

*barzakh@mail.ru

in contrast to the spherical ground states with $I^\pi = 1/2^+$ (see Ref. [1] and references therein). This interpretation is supported by the isotope and isomer-shift measurements which provide evidence for the marked difference between the radii for the ground and the isomeric (intruder) states in the odd-A $^{185-197}$Tl (see Ref. [7] and references therein). This difference is explained by the corresponding change in quadrupole deformation. Following Refs. [3,9], the appearance of two $9/2^-$ low-lying states, based on prolate and oblate configurations, respectively, is expected around ^{183}Tl. Their mixing might lead to a change in radii of the observed $9/2^-$ intruders, which can be probed in laser spectroscopy experiments.

In the odd-odd Tl isotopes, the coupling of both normal $\pi 3s_{1/2}$ and intruder $\pi 1h_{9/2}$ orbitals with valence neutrons from several shells should be considered. In particular, long-lived high-spin intruder states of presumably $[\pi 1h_{9/2} \times \nu 1i_{13/2}]_{7^--10^-}$ origin are well known in the odd-odd $^{184-200}$Tl isotopes, and their tentative spin-parity assignments are based on decay spectroscopy experiments [2,10]. So far, laser spectroscopy studies of these isomers have been restricted to ^{186}Tl only [7]. In Ref. [7] the configuration assignment of $[\pi 1h_{9/2} \times \nu 1i_{13/2}]_{10^-}$ was confirmed, and a large difference in the charge radii between the intruder isomer and the ground state was observed. The further study of Tl intruder isomers (both odd A and even A) towards the more neutron-deficient region are of particular importance for the investigation of their expected change in structure due to the mixture of the two $(9/2^-)$-based bands [3,9].

The isotope shift and hyperfine structure investigations presented in this paper are a part of an experimental campaign at the Isotope Separator On-Line (ISOLDE) facility (CERN) aimed at dedicated β-delayed fission, nuclear decay, and laser spectroscopy studies of the neutron-deficient thallium isotopes. Partial results for β-delayed fission and nuclei decay spectroscopy measurements of ^{178,180,182,184}Tl are reported in Refs. [11–14].

II. EXPERIMENTAL DETAILS

We outline here only the basic principles of the experimental setup and the measurement procedure; a detailed description can be found in Ref. [15].

The experiments were performed at the ISOLDE facility (CERN) [16]. Radioactive Tl isotopes are produced in spallation reactions by a 1.4-GeV proton beam (intensity up to 2 μA) from the CERN PS booster in a 50 g/cm^2 UC_x target. The spallation products diffuse out of the high-temperature target material as neutral atoms and effuse into the cavity of the Resonance Ionization Laser Ion Source [17]. Laser beams are introduced into this cavity through a fused silica window and, for this paper, the lasers were tuned to perform two-step resonance ionization of Tl atoms via the following scheme:

$$6p\ ^2P_{1/2} \xrightarrow[\text{NBL}]{276.9\,\text{nm}} 6d\ ^2D_{3/2} \xrightarrow[\text{Nd:YAG}]{532\,\text{nm}} \text{continuum}.$$

The excitation from the atomic ground-state $6p\ ^2P_{1/2}$ to an intermediate electronic state $6d\ ^2D_{3/2}$ (36 117.9 cm^{-1}) was performed by a frequency-doubled narrow-band tunable dye laser (NBL) beam at 276.9 nm with a linewidth of about 0.8 GHz (before frequency doubling). Pumping of the dye laser and subsequent ionization of the excited thallium atoms was accomplished using the 532-nm output of a 10-kHz EdgeWave Nd:YAG (where YAG represents yttrium-aluminum-garnet) laser. The average power of the laser beams injected into the 3-mm diameter aperture of the ion source cavity was up to 70 mW at 276.9 nm and 17 W at 532 nm. During the IS and hfs measurements the laser power for the first excitation step was reduced to a few milliwatts to avoid saturation broadening of the spectral line.

After selective laser photoionization, the radioactive thallium ions were extracted and accelerated to 50 kV, separated in mass with the General Purpose Separator of ISOLDE and directed to the counting stations: either a Faraday cup (FC) or Windmill (WM) setup [14]. For the stable isotopes ^{203,205}Tl, which were evaporated into the ion source cavity from a dedicated oven, a direct measurement of the ion current by a Faraday cup was used.

At the WM setup, the mass-separated ions of the short-lived isotopes $^{179-184}$Tl were implanted into one of ten carbon foils (20 μg/cm^2 thickness) mounted on a rotating wheel. The photoion current was measured via the detection of characteristic β-γ and/or α decays of the isotopes in question as a function of the scanned laser frequency of the first excitation step. For α-decay detection, the implantation foil was surrounded by two circular silicon detectors, one of which was of an annular type that allowed the beam to pass through its center. To detect γ rays, two single-crystal high-purity germanium detectors were placed outside the vacuum chamber. A detailed description of the Windmill setup is given in Refs. [14,15].

Figure 1 shows examples of the hfs spectra for several thallium isotopes. The dependence of their count rate (measured either in FC or in WM) is plotted as a function of the frequency of the scanned narrow-band laser. In some cases, to increase the statistics in the hfs spectrum, α decays of daughter products (Hg, Pt, and Au after β and α decays) also were taken into account (see additional examples of hfs spectra in Fig. 1, Ref. [13]).

III. DATA ANALYSIS

The positions of the hyperfine components as a function of the scanning laser frequency are determined by the formulas [18],

$$\nu^{F,F'} = \nu_0 + \Delta\nu^{F'} - \Delta\nu^{F},$$

where ν_0 is the position of the center of gravity of the hfs, the prime symbol denotes the upper level of the atomic transition, and

$$\Delta\nu^{F} = a\frac{K}{2} + b\frac{0.75 \times K(K+1) - I(I+1)J(J+1)}{2(2I-1)(2J-1)IJ}, \quad (1)$$

where $K = F(F+1) - I(I+1) - J(J+1)$, F is the total angular momentum of the atomic level, and a and b are the magnetic dipole and electric quadrupole hyperfine coupling constants, respectively. These constants are proportional to

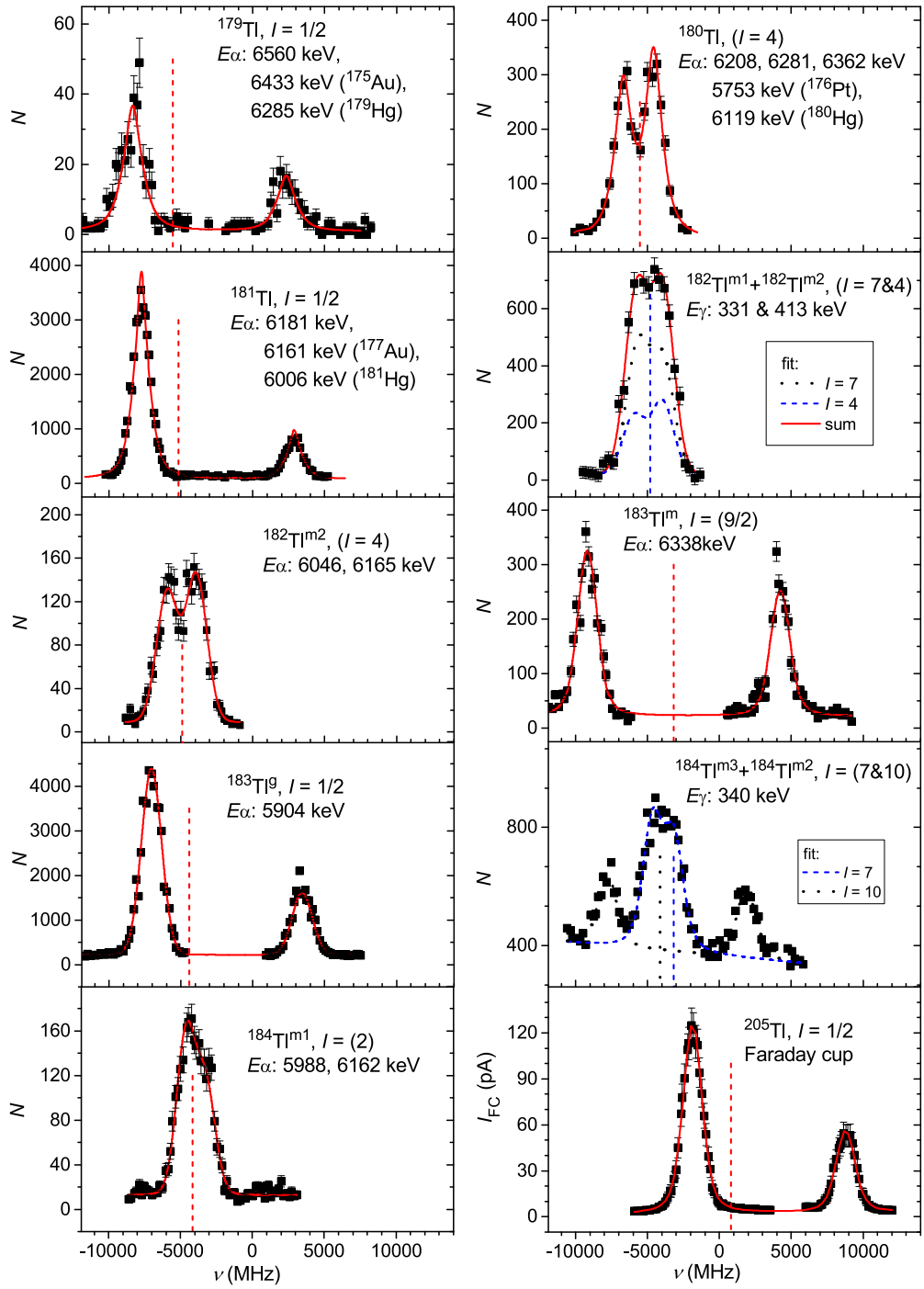

FIG. 1. The hfs spectra of selected Tl isotopes. In the insets the spin of the corresponding nuclide and the energies of the γ- or α-decay lines used for the photoion current monitoring are shown. The solid lines depict the Voigt-profile fit to the data. The vertical dashed lines mark the center of gravity of the corresponding hfs. The zero point on the frequency scale corresponds to a wave number of 18 059.0 cm^{-1}.

the nuclear magnetic dipole (μ) and electric quadrupole (Q_s) moments, respectively.

Experimental hfs spectra were fitted by the Voigt profile. In the fitting procedure the ratio a'/a was fixed in accordance with its value for the stable isotope ^{205}Tl: $a(6d\,^2D_{3/2}, {}^{205}\mathrm{Tl})/a(6p\,^2P_{1/2}, {}^{205}\mathrm{Tl}) = -0.002\,013(19)$ [19]. The details of the fitting procedure can be found in Ref. [7].

In the fitting procedure the nuclear spin should be fixed. Spins $I = 1/2$ for the ground states in ^{179,181,183}Tl were determined by the hfs pattern analysis (see Sec. IV). For other Tl nuclei a comparison of the fits with different spin assignments does not enable a definite conclusion about the "best-suited" spin. Tentative spin assignments, based on (α/β)-decay systematics, were proposed for ^{180,182,184}Tl in Refs. [12–14,20]. Some of these were substantiated by the

TABLE I. Isotope shifts, $\delta\nu_{205,A}$, and magnetic hfs constants a determined in the present paper. Respective literature data where known are shown in the last two columns.

A	I	$\delta\nu_{205,A}$ (MHz)	$a(6p\,^2P_{1/2})$ (MHz)	$\delta\nu_{205,A}$ (MHz), literature	$a(6p\,^2P_{1/2})$ (MHz), literature
205	1/2	0	21290(70)	0	21310.835(5)[a]
203	1/2	−1004(140)	21020(100)	−1038.5(1)[b]	21105.447(5)[a]
184m1	(2)[c]	−9930(320)	1045(110)	−10070(300)[d]	1030(320)[d]
184m2	(7)[c]	−9890(240)	399(18)		
184m3	(10)[c]	−7960(210)	1820(50)		
183m	(9/2)[e]	−7960(160)	5268(80)		
183g	1/2	−10460(160)	20868(90)	−10690(270)[d]	21060(480)[d]
182m1	(4)[f]	−11340(180)	−900(50)		
182m2	(7)[f]	−11370(310)	508(90)		
181	1/2	−11890(160)	21321(180)		
180 ($I=4$)	(4)[g]	−12680(220)	−919(34)		
180 ($I=5$)	(5)[g,h]	−12730(220)	−755(30)		
179	1/2	−12900(290)	21310(200)		

[a]Reference [21].
[b]Reference [19].
[c]References [13,14].
[d]Reference [7].
[e]Reference [22].
[f]Reference [14] and the present paper.
[g]Reference [12].
[h]Reference [20].

magnetic moment analysis in the present paper (see Sec. V). During the fitting, spins for these nuclides were fixed in accordance with adopted assignments (see Table I). The ordering of the long-lived states in ^{182,184}Tl is unknown, thus they are denoted by "m1" and "m2" in the present paper. For the ground state of ^{180}Tl a tentative assignment $I=(4,5)$ was proposed on the basis of our β-decay study [12], whereas $I=(5)$ was proposed in Ref. [20]. Correspondingly, both options were used in the ^{180}Tl-hfs fitting (see Table I). In columns 5 and 6 of Table I isotope shift and hfs constants obtained previously [7,19,21] are presented. They agree fairly well (within the experimental uncertainties) with the present data.

IV. RESULTS

A. Spins and magnetic moments

Due to the low electronic spin ($J=1/2$) of the atomic ground state in thallium, nuclear spins for the investigated nuclei cannot be determined by counting of the hyperfine components [18]. On the other hand, the nuclear spin determines the shape of the hfs spectra, in particular, the amplitude ratio of the two observed hyperfine components. In the case of odd-A ^{179,181,183}Tl ground states, a good fit of the hfs can only be achieved with a spin assignment of $I=1/2$. As an example, in Fig. 2 the hfs fits obtained with the nuclear spin assumptions of $I=1/2$ and $3/2$ are compared. This comparison demonstrates the strong preference for the former value. Other spin assignments ($I=5/2, 7/2$, etc.) give even worse descriptions of the observed hfs. Thus, the nuclear spin $I=1/2$ was unambiguously determined for ^{179,181,183}Tl^g in our experiment.

For the evaluation of the magnetic moments, the following relation [18] was used:

$$\mu_A=\mu_{A_0}\frac{I_A}{I_{A_0}}\frac{a_A(6p\,^2P_{1/2})}{a_{A_0}(6p\,^2P_{1/2})}[1+{}^{A_0}\Delta^A(6p\,^2P_{1/2})], \qquad (2)$$

where ${}^{A_0}\Delta^A(nl)$ is the hyperfine structure anomaly (HFA) [23].

It was shown in Ref. [24], that the relativistic "coupled-cluster" approach [25] describes experimental data for the HFA in thallium fairly well. This approach was used in Ref. [7] for the estimation of the HFA for Tl isotopes with spins $I=1/2,9/2,2,10$: ${}^{205}\Delta^A(6p\,^2P_{1/2}; I=1/2)=-6(4)\times10^{-4}$; ${}^{205}\Delta^A(6p\,^2P_{1/2}; I=9/2)=-7(2)\times10^{-3}$; ${}^{205}\Delta^A(6p\,^2P_{1/2}; I=2)=-1(7)\times10^{-3}$; ${}^{205}\Delta^A(6p\,^2P_{1/2};$

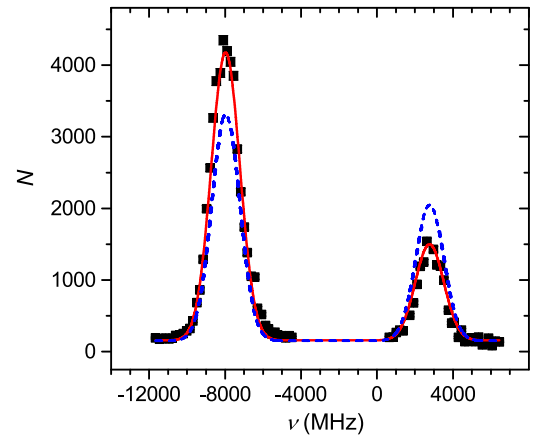

FIG. 2. Hyperfine structure spectrum of ^{181}Tl^g. The full line represents fitting with $I=1/2$, and the dashed line represents fitting with $I=3/2$.

TABLE II. Magnetic moments and changes in mean-square charge radii for Tl nuclei.

A	I	$\mu(\mu_N)$	$\delta\langle r^2\rangle_{205,A}$ (fm^2)[a]
184m1	(2)	0.321(36)	−0.979(32) {69}
184m2	(7)	0.428(22)	−0.976(24) {68}
184m3	(10)	2.778(78)	−0.777(20) {54}
183m	(9/2)	3.619(62)	−0.775(15) {54}
183g	1/2	1.603(8)	−1.033(15) {72}
182m1	(4)	−0.549(33)	−1.120(18) {78}
182m2	(7)	0.54(10)	−1.123(30) {78}
181	1/2	1.638(14)	−1.174(16) {82}
180	(4)	−0.564(23)	−1.254(22) {88}
179	1/2	1.637(16)	−1.274(29) {89}

[a]The errors in parentheses are the statistical experimental uncertainties. The systematic errors are given in curly brackets and stem from the uncertainty of the F and M factors.

$I = 10) = -7.1(6) \times 10^{-3}$. By using the same approach, the HFA corrections for Tl nuclei with spins $I = 4,5,7$ were calculated in the present paper: $^{205}\Delta^A(6p\ ^2P_{1/2}; I = 4) = -2(4) \times 10^{-3}$; $^{205}\Delta^A(6p\ ^2P_{1/2}; I = 5) = -2(4) \times 10^{-3}$; $^{205}\Delta^A(6p\ ^2P_{1/2}; I = 7) = -4(6) \times 10^{-3}$.

These values were used here for the evaluation of the magnetic moments. In Table II the magnetic moments of the Tl isotopes corrected by the estimated HFA are presented. In Ref. [26] the HFA for the Tl isotopes was estimated by the application of the empirical Moskowitz-Lombardi rule [27]. However, it was shown recently [28] that this rule is not universal and should be applied to the HFA estimation with caution.

B. Changes in mean-square charge radii

The changes in the mean-square charge radii $\delta\langle r^2\rangle^{A,A'}$ were deduced from the measured isotope shifts $\delta\nu^{A,A'}$ using the relations [18],

$$\delta\nu^{A,A'} = F_\nu\lambda^{A,A'} + M_\nu\frac{A-A'}{AA'}, \tag{3}$$

where $M_\nu = M_\nu^{\rm NMS} + M_\nu^{\rm SMS}, M_\nu^{\rm NMS} = \frac{\nu}{(m_p/m_e)}, \lambda^{A,A'} = K(Z)\delta\langle r^2\rangle^{A,A'}$, ν is the transition frequency, $M_\nu^{\rm NMS}$ and $M_\nu^{\rm SMS}$ are normal mass shift (NMS) and specific mass shift (SMS) constants, respectively, and $K(Z)$ takes into account the contribution of the higher-order radii moments in $\lambda^{A,A'}$ (see Ref. [29]).

The values $F_{535\,\rm nm} = -18.0\,\rm GHz\,fm^{-2}$ and $M_{535\rm nm}^{\rm SMS} = 0\,\rm GHz\,amu$ were used in Ref. [30] in a combined analysis of the optical, the muonic atom, and the electron-scattering data in a model-independent way. The contribution of the higher-order radii moments was also determined in this analysis: $K(81) = 0.938$. The assumption of zero SMS is justified by the estimation of SMS for some Tl levels in the framework of many-body perturbation theory [31]. These values of $F_{535\,\rm nm}$, $M_{535\,\rm nm}$, and $K(81)$ were used in Ref. [7] in a King-plot procedure [18] to determine atomic F and M constants for the 276.9-nm transition: $F_{276.9\,\rm nm} = 10.38\,\rm GHz\,fm^{-2}$ and $M_{276.9\,\rm nm} = 701\,\rm GHz\,amu$. A scaling uncertainty due to F and M indeterminacies can be estimated as 7% (see Ref. [18]). In Table II, the values of $\delta\langle r^2\rangle_{205,A}$ deduced from the IS data by Eq. (3) with the atomic constants for the 276.9-nm transition are presented. The errors in parentheses reflect only the statistical isotope shift uncertainties; the systematic errors which stem from the scaling uncertainty of the electronic factor and the specific mass shift are given in curly brackets.

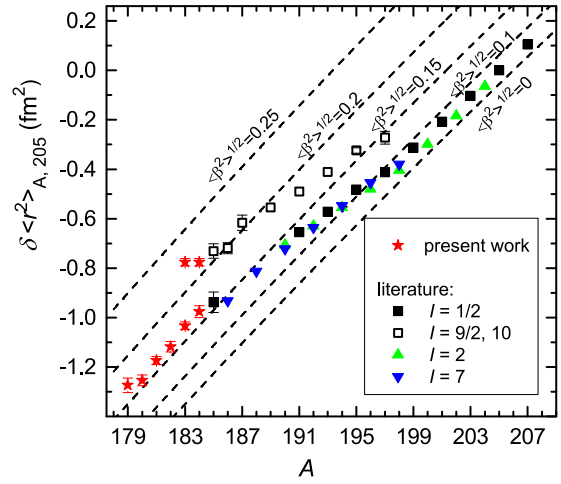

FIG. 3. Isotopic dependence of the changes in the mean-square charge radii for the Tl isotopes. Present data are marked by the star symbols. Literature data are taken from Ref. [7] (see also references therein). Full squares: ground states with $I = 1/2$; hollow squares: intruder isomers [$I = (9/2), (10)$]; upward triangles: nuclei with $I = (2)$; downward triangles: nuclei with $I = (7)$. The dashed lines represent the droplet model prediction with different constant mean-square deformations. Only statistical errors are displayed.

Figure 3 shows the changes in the mean-square charge radii $\delta\langle r^2\rangle_{205,A}$ of the Tl nuclei. For ^{183}Tl the $\delta\langle r^2\rangle$ value measured in the present paper is shown since it has a smaller error than the value obtained in Ref. [7]. As is seen in Table II, the radii for $^{184}\rm Tl^{m1}$ [$I = (2)$] and $^{184}\rm Tl^{m2}$ [$I = (7)$] are the same within the experimental uncertainties and would be indistinguishable in Fig. 3, therefore only the $\delta\langle r^2\rangle(^{184}\rm Tl^{m2})$ is shown. The same is true for $^{182}\rm Tl^{m1}$ [$I = (4)$] and $^{182}\rm Tl^{m2}$ [$I = (7)$], which is why only the $\delta\langle r^2\rangle$ value for $^{182}\rm Tl^{m2}$ [$I = (7)$] is shown in this case.

It is generally acknowledged that the main isotopic trend of the $\delta\langle r^2\rangle$ values is described by the droplet model (DM) (see Ref. [32] and references therein). Deviations from the DM trend can be attributed to the development of the mean-square quadrupole deformation according to the expression,

$$\langle r^2\rangle = \langle r^2\rangle_{\rm DM}\left(1 + \frac{5}{4\pi}\langle\beta_{\rm DM}^2\rangle\right), \tag{4}$$

where $\langle r^2\rangle_{\rm DM}$ is the mean-square charge radius calculated by the DM with zero deformation. In Fig. 3, the lines of $\delta\langle r^2\rangle$ calculated with the DM parameters from Ref. [32] and a constant mean-square deformation (setting $\langle\beta^2\rangle^{1/2}(^{205}\rm Tl) = \langle\beta^2\rangle^{1/2}(^{204}\rm Hg) = 0.069$ [33]) are also shown to provide insight into the development of the deformation across the Tl isotopic chain.

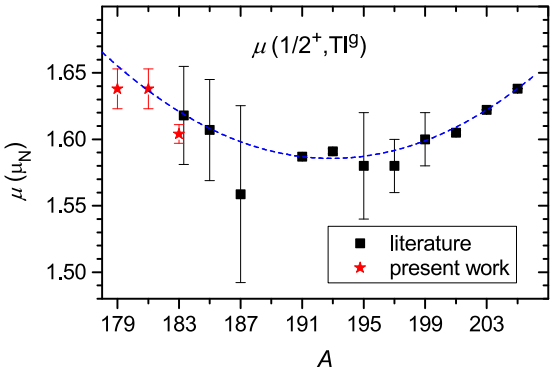

FIG. 4. Magnetic moments for the Tl^g ($I = 1/2$) isotopes. Squares: literature data (see Ref. [7] and references therein). Stars: present paper. A parabolic fit is shown by the dashed curve.

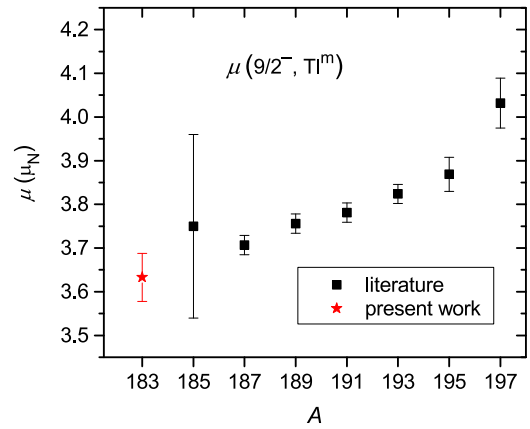

FIG. 5. Magnetic moments for Tl^m ($I = 9/2$) isotopes. Squares: literature data (Ref. [7] and references therein). Star: present paper.

Section V B provides a detailed discussion of the $\delta\langle r^2\rangle$ behavior in the Tl isotope chain.

V. DISCUSSION

A. Spins and magnetic moments

In this section we discuss the systematics of the spins and magnetic moments of the neutron-deficient Tl isotopes. The discussion of the magnetic moments of the odd-odd Tl isotopes is guided by comparisons with estimates from the additivity relation to obtain information on the underlying configuration.

1. Odd-A isotopes

Figure 4 shows the magnetic moments for Tl isotopes with $I = 1/2$. The known value for ^{207}Tl ($1.88\mu_N$) is not shown in the plot to avoid a strong compression of the Y scale. Despite the rather large errors for ^{185,187,195}Tl, the measured magnetic moments clearly follow a parabolic A dependency with a minimum near $A = 191$.

The strong decrease in magnetic moment from $1.88\mu_N$ for ^{207}Tl to $1.64\mu_N$ for ^{205}Tl has been previously explained by a noticeable change in the second-order core-polarization effects, in this case, the mixture with particle-core-coupled configurations in which a valence nucleon couples to the first excited 2^+ core state [34,35]. The main contribution to this effect is expected to be due to the change in the admixture of the $(2^+ \times \pi d_{3/2})_{1/2+}$ state because of the jump of the lowest 2^+ state from 4.1 MeV in ^{208}Pb to a smaller value around ≈0.9 MeV for the lighter even-N core Pb isotopes. However, the same mechanism cannot be responsible for the observed parabolic A dependency of the $\mu(1/2^+,Tl^g)$ values. The change in the second-order core-polarization correction caused by the $[2^+(\text{Pb core}) \times \pi d_{3/2}]_{1/2+}$ state admixture is determined principally by the changes in the energy of the core 2^+ state and $3/2^+$ state in the odd-mass Tl isotopes [35]. However, the energy of the 2^+_1 state in the core Pb nuclei and the energy of the Tl $3/2^+$ state slowly increase with the decrease in A (until $N = 114$) (see Ref. [36] and references therein). Correspondingly, the aforementioned second-order core-polarization correction should decrease until $A = 196$, which contradicts the observed A dependence of the $1/2^+$ magnetic moments. Evidently, other possible mechanisms should be taken into account (for example, $\pi s_{1/2}$ coupling with the 0^+_2 core intruder state, etc.). Although a full understanding of the observed behavior needs further theoretical work, it is intriguing that this behavior follows the "typical" parabolic trend of the intruder state energy in the lead and neighboring nuclei (see Ref. [37] and references therein).

In contrast to the parabolic behavior of the $\mu(1/2^+,Tl^g)$ values, the magnetic moments of the Tl intruder isomers with $I = (9/2)$ follow a linearly decreasing A dependence (see Fig. 5), approaching more closely the Schmidt value ($\mu_{\text{Schmidt}} = 2.6\mu_N$) when going away from the closed shell.

2. ^{180}**Tl** ***(N = 99)***

So far, only one long-lived state, assumed to be the ground state, was found in ^{180}Tl (see dedicated α- and β-decay studies [12,20]). An examination of the hfs patterns for different γ-ray and α-decay transitions, associated with the ^{180}Tl decay, did not reveal any indication of another long-lived state in ^{180}Tl, in agreement with the results of the decay studies.

In Ref. [12] a tentative spin-parity assignment of $I^\pi(^{180}Tl^g) = (4^-,5^-)$ was proposed with the most probable configuration of $[\pi 3s_{1/2} \times \nu 1h_{9/2}]$. This assignment was based on the ^{180}Tl β-decay pattern with the dominant feeding to the 4^+ state in the daughter ^{180}Hg and an additional feeding to the 5^- and 6^+ states. In the α-decay study of ^{180}Tl [20] the $I^\pi(^{180}Tl^g) = (5^-)$ assignment with the same $[\pi 3s_{1/2} \times \nu 1h_{9/2}]$ configuration as in Ref. [12], was proposed. Apart from the (β/α)-decay pattern arguments, the configuration assignment in Refs. [12,20] was based on the expected complete depletion of the $1i_{13/2}$ neutron shell below ^{181}Tl ($N = 100$) with the $1h_{9/2}$ (or possibly, $2f_{7/2}$) neutron orbital starting to play a role in the lightest Tl isotopes with $N < 100$. In this respect it is relevant to notice that the ground state of the $N = 99$ isotone ^{181}Pb was indeed assigned as $I^\pi = 9/2^-$ of the $\nu 1h_{9/2}$ configuration (Ref. [38]; see also Ref. [39]), whereas the ground state and the first excited state in the $N = 99$ isotone ^{179}Hg were interpreted as $\nu 2f_{7/2}$ and $\nu 1h_{9/2}$ states, respectively (see Refs. [40,41] and references therein).

TABLE III. Comparison of the experimental magnetic moments $\mu_{\rm exp}$ for ^{180}Tl^{g} obtained with different spin and configuration assumptions with magnetic moments $\mu_{\rm add}$ calculated by the additivity relation.

Configuration	Spin	$\mu_{\rm add}(\mu_N)$	$\mu_{\rm exp}(\mu_N)$
$\pi 3s_{1/2} \times \nu 1h_{9/2}$	4	−0.58	−0.564(23)
$\pi 3s_{1/2} \times \nu 1h_{9/2}$	5	2.38	−0.579(24)
$\pi 3s_{1/2} \times \nu 2f_{7/2}$	4	0.70	−0.564(23)

We have investigated the inference on the possible spin and configuration of ^{180}Tl which can be drawn from the magnetic moment values determined in the present paper. Following the discussion above, we will consider two possible configurations $[\pi 3s_{1/2} \times \nu 2f_{7/2}]_{4-}$ and $[\pi 3s_{1/2} \times \nu 1h_{9/2}]_{4-,5-}$, which can both explain the proposed spin $I^{\pi}(^{180}\mathrm{Tl}^{g}) = (4^{-})$, whereas only the latter can explain $I^{\pi}(^{180}\mathrm{Tl}^{g}) = (5^{-})$.

According to the additivity relation [26], the magnetic moment of a two-particle state $|i_p i_n I\rangle$ in an odd-odd nucleus can be calculated from the following formula:

$$\mu_{\rm add} = \frac{I}{2}\left(\frac{\mu_p}{i_p} + \frac{\mu_n}{i_n}\right) + \frac{I}{2}\left(\frac{\mu_p}{i_p} - \frac{\mu_n}{i_n}\right) \times \frac{i_p(i_p+1) - i_n(i_n+1)}{I(I+1)}, \quad (5)$$

where i_p and i_n are the proton and neutron single-particle angular moments; μ_p and μ_n are the single-particle magnetic moments. For the latter values, the known magnetic moments of the adjacent odd-A nuclei can be used. Our experimentally determined magnetic moment was used for the $3s_{1/2}$ proton: $\mu_p(\pi 3s_{1/2}) = \mu(^{181}\mathrm{Tl}_{100}) = 1.64\mu_N$ (see Table II), and a value of $\mu_n(\nu 2f_{7/2}) = \mu(^{179}\mathrm{Hg}_{99}) = -0.94\mu_N$ from Ref. [42] also was used.

As there are no experimental data for the magnetic moment of the $1h_{9/2}$ neutron state (e.g., for ^{181}Pb), $\mu_n(\nu 1h_{9/2})$ was calculated by the standard single-particle formula,

$$\mu(I) = I[g_l \pm (g_s - g_l)/(2l+1)] \quad \text{for } I = l \pm 1, \quad (6)$$

where g_l and g_s are orbital and spin g factors. In a nucleus, the magnetic moments of the proton and neutron are influenced by the medium, therefore one usually uses "effective" proton and neutron g factors to calculate the single-particle moments. From a comparison with the different experimental data the following renormalization of neutron g factors in the lead region was proposed: $g_s = 0.6 g_{s,\,\rm free}$, $g_l = -0.04$ (Ref. [43]; see also the discussion in Ref. [44]). With this renormalization Eq. (6) gives: $\mu_n(\nu 1h_{9/2}) = 0.74\mu_N$.

In Table III, the $\mu(^{180}\mathrm{Tl}^{g})$ values calculated by Eq. (5) with different spin and configuration assumptions are compared with the experimental values. Only the $[\pi 3s_{1/2} \times \nu 1h_{9/2}]_{4^-}$ configuration matches the observed negative experimental value, whereas other variants can be rejected as they do not reproduce the negative sign of the magnetic moment. Thus, this comparison strongly supports the $I^{\pi}(^{180}\mathrm{Tl}^{g}) = (4^{-})$ assignment with the dominant configuration $[\pi 3s_{1/2} \times \nu 1h_{9/2}]$.

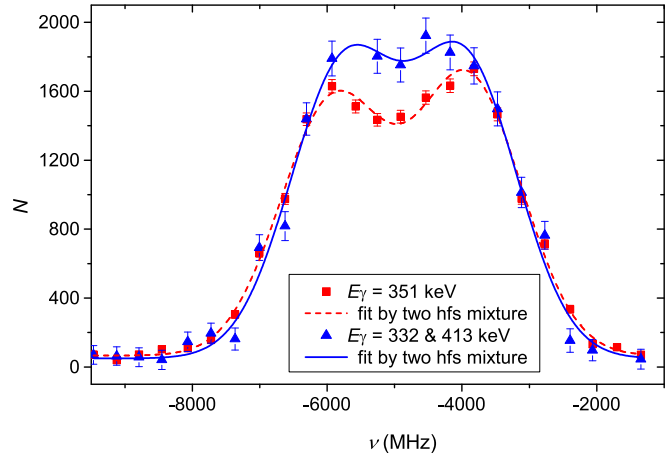

FIG. 6. Hyperfine structure pattern for different γ lines in the ^{182}Tl β decay: squares: $E_\gamma = 351$ keV; triangles: $E_\gamma = 413$ and 332 keV (multiplied by 2.6). The solid and dashed lines represent the fits by the two hfs mixtures.

The reasonable variations in the values used for the effective g factors do not alter this conclusion.

3. ^{182}Tl ($N = 101$)

In Ref. [45] a (7^{+}) assignment for the ^{182}Tl parent state with a half-life of 3.1(10) s was proposed based on the observed population in its β decay of the levels up to 8^{+} in the daughter nuclide ^{182}Hg. In the α-decay study of ^{186}Bi [46], evidence was found for the presence of two [low-spin (ls) and high-spin (hs)] long-lived states in ^{182}Tl. As no information on their relative position is yet known, they will be denoted below as high-spin and low-spin isomers.

The hyperfine structure patterns for different α and γ lines in the ^{182}Tl decay spectra, obtained in narrow-band laser scans, strongly support the presence of two long-lived states in ^{182}Tl. This is seen, for example, in Fig. 6 which shows that the hfs patterns observed in the laser scans when gating on the $8^{+} \rightarrow 6^{+}$ (413-keV) and $6^{+} \rightarrow 4^{+}$ (332-keV) transitions in ^{182}Hg are distinctly different from the pattern corresponding to the $2^{+} \rightarrow 0^{+}$ (351-keV) transition. For the sake of brevity the observed dependence of the intensity of γ or α line with the energy E on the laser frequency will be denoted as E-hfs (for example, 351-hfs, and so on). The hfs scans corresponding to the low- or high-spin isomer will be denoted as ls-hfs or hs-hfs, respectively.

It is reasonable to suppose that the 8^{+} and 6^{+} levels in ^{182}Hg are predominantly fed by the β decay of the high-spin (presumably, 7^{+}) isomer of ^{182}Tl. Correspondingly, the relative contribution of the hs-hfs to the 413 and 332-hfs ($8^{+} \rightarrow 6^{+}$ and $6^{+} \rightarrow 4^{+}$ transitions in ^{182}Hg) compared to the ls-hfs should be larger than in the case of 351-hfs ($2^{+} \rightarrow 0^{+}$ transition). This explains the difference among 413, 332, and 351-hfs since hs-hfs and ls-hfs are expected to have different shapes (see the fits in Fig. 6).

From the analysis of the hfs patterns for different γ lines, one can conclude that ls-hfs represents two not fully resolved peaks with a clear dip in the center, whereas hs-hfs

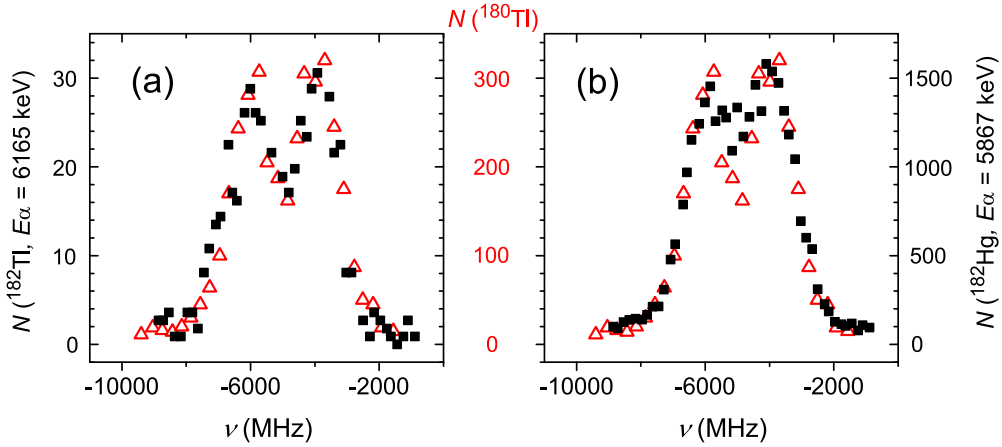

FIG. 7. Comparison of the hfs patterns for ^{180}Tl (triangles: the same data as in Fig. 1) and for ^{182}Tl (squares), deduced (a) via the 6165-keV α-decay line of ^{182}Tl and (b) via the 5867-keV α-decay line of the daughter isotope ^{182}Hg. The data for ^{180}Tl are shifted by 670 MHz to overlap the data of both isotopes.

represents one broad flattopped peak. In the β-decay study of the same data set [47], a noticeable population of the 4_1^+ ($E^* = 612$-keV) and 4_2^+ ($E^* = 1124$-keV) states in the daughter ^{182}Hg was observed along with the previously found 6^+ and 8^+ feedings [45]. This also points to the presence of two long-lived states in ^{182}Tl: high spin (presumably, 7^+) and low spin (presumably, $I = 3$–5).

In our dedicated α-decay study of ^{182}Tl, several ^{182}Tl α-decay lines were observed [14]: $E_\alpha = 5962$, 6046, 6165, 6406, and 6360 keV. Remarkably, the 6165-hfs and 6046-hfs patterns practically coincide with the hfs pattern of ^{180}Tl, see Fig. 7(a) where the 6165-hfs is compared with the hfs of ^{180}Tl (deduced via α decay). Correspondingly, one can suppose that at least the 6165-hfs and 6046-hfs are pure, i.e., in these cases the contribution of the hs-hfs is negligible. At the same time, the similarity of the hfs patterns of the low-spin ^{182}Tl isomer (6165-hfs and 6046-hfs) and of ^{180}Tl suggests that the same $[\pi 3s_{1/2} \times \nu 1h_{9/2}]_{4^-}$ configuration is involved in both cases. This tentative spin assignment for the low-spin isomer in ^{182}Tl was further used in the fitting procedure. A definite conclusion on the hfs pattern for other ^{182}Tl α lines, found in Ref. [14], cannot be made owing to the low intensity of these lines, although the dip between the two hfs peaks in the corresponding spectra testifies to the predominance of the low-spin state as the origin of these α lines.

The (7^+) spin and parity assignment for the high-spin isomer in ^{182}Tl is compatible with the corresponding assignment for one of the long-lived states in the heavier isotopes $^{186-204}$Tl (see Ref. [8] and references therein). This tentative spin assignment for the high-spin isomer was used in the fitting procedure.

In contrast to the pure low-spin character of the hfs produced by the intense ^{182}Tl α lines, the hfs of the $E_\alpha =$ 5867-keV α-decay line of the daughter ^{182}Hg testifies to the presence of contributions of both isomers in this hfs, which is consistent with the production of ^{182}Hg in the β decays of both isomers [see Fig. 7(b)].

The presence of two strongly overlapping hfss in the laser scans demands the application of a "two-hfs" fitting model which takes into account a possible mixture of two sets of hyperfine components with different I, a, and ν_0 parameters [cf. Eq. (1)] and the same linewidths. All hyperfine spectra produced for different α or γ lines, could be consistently fitted by this two-hfs fitting model (see examples in Fig. 6). The resulting magnetic moment for the presumed 7^+ state, $\mu(7^+, {}^{182}\mathrm{Tl}^{m2}) = 0.54(10)\mu_N$, follows the general trend of magnetic moments of the states with the same spin in the heavier Tl nuclei. The magnetic moment of the presumed 4^- state, $\mu(4^-, {}^{182}\mathrm{Tl}^{m1}) = -0.549(33)\mu_N$, coincides, within the experimental uncertainties, with the magnetic moment of ^{180}Tl^g with the same (presumed) configuration and spin. These observations support the applicability of the fitting procedure used for the description of the mixed hfs spectra and point to the consistency of the supposed assignments.

4. ^{184}Tl ($N = 103$)

Based on the observed feeding to the excited 8^+ and 2^+ states in the daughter isotope ^{184}Hg, two β-decaying states in ^{184}Tl were identified [48] with proposed spin and parity (7^+) and (2^-). They are understood as being due to normal $[\pi 3s_{1/2} \times \nu 1i_{13/2}]_{7^+}$ and $[\pi 3s_{1/2} \times \nu 3p_{3/2}]_{2^-}$ configurations, similar to the analogous states in some of the heavier odd-odd Tl isotopes. In the α-decay study of ^{188}Bi [10], an additional long-lived (10^-) state at 500(5) keV above the (7^+) state was found and assigned to an intruder $[\pi 1h_{9/2} \times \nu 1i_{13/2}]_{10^-}$ state. In our subsequent experiments at ISOLDE, the excitation energy of the 10^- isomer was measured with an improved precision as 506.1(1) keV, and its half-life of 47.1(7) ms was determined for the first time [13].

Following the example of ^{180}Tl in Sec. V A 2, it is instructive to compare experimental magnetic moments with the additivity relation predictions [Eq. (5)] to check the configuration assignments in ^{184}Tl. The magnetic moment for the $[\pi 1h_{9/2} \times \nu 1i_{13/2}]_{10^-}$ configuration in ^{184}Tl was calculated with the values of $\mu_p(\pi 1h_{9/2}) = \mu({}^{183}\mathrm{Tl}^m) = 3.618(55)\,\mu_N$ (see Table II) and $\mu_n(\nu 1i_{13/2}) = \mu({}^{193}\mathrm{Po}^m) = -0.742(65)\,\mu_N$ taken from Ref. [15]. It should be noted that the magnetic moment of the neutron 13/2 state grows rapidly when the

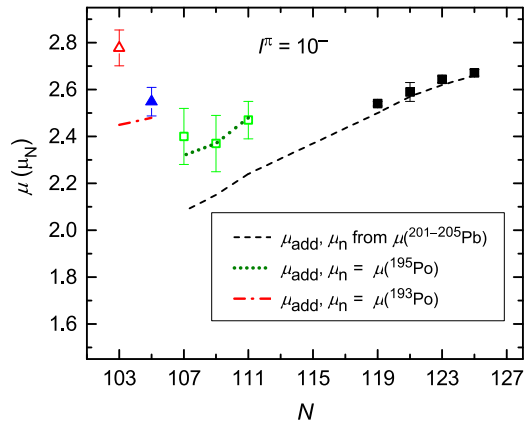

FIG. 8. Magnetic moments of Tl and Bi isomers with $I = 10$. Squares: Bi isomers (full squares: Ref. [49]; hollow squares: Ref. [50]). Triangles: Tl isomers (hollow triangle: present paper; full triangle: Ref. [7]). The results of a calculation using the additivity relation [Eq. (5)] with different assumptions for μ_n are shown by lines (see the text for details).

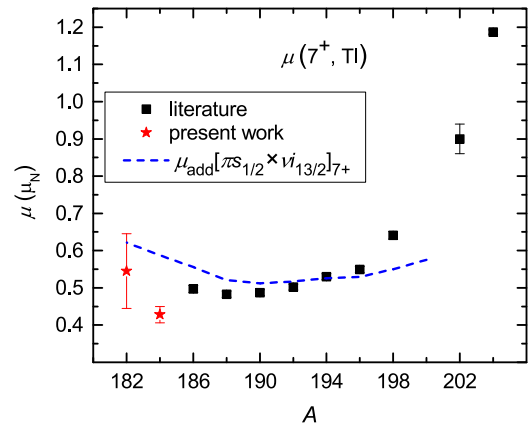

FIG. 9. Magnetic moments for Tl isotopes with $I = 7$. Squares: literature data (see Ref. [7] and references therein). Stars: present paper. Dashed line: calculation by the additivity relation [Eq. (5)] with μ_p and μ_n values from experimental magnetic moments of the adjacent odd-A nuclei.

deformation increases [15]. Therefore it would be misleading to use magnetic moments of adjacent ^{185}Hg or ^{185}Pb as $\mu_n(\nu 1i_{13/2})$ for the $\mu_{add}(10^-, ^{184}Tl)$ calculation since these isotopes have a mean-square deformation of only $\langle\beta^2\rangle^{1/2}(^{185}Hg) = 0.16(1)$ [4] and $\langle\beta^2\rangle^{1/2}(^{185}Pb) \approx 0.1$ [6], both markedly lower than the mean-square deformation of the $[\pi 1h_{9/2} \times \nu 1i_{13/2}]$ intruder state in ^{184}Tl, $\langle\beta^2\rangle^{1/2}(^{184}Tl, 10^-) = 0.22(2)$ (see Fig. 3). At the same time, the mean-square deformation of ^{193}Po, $\langle\beta^2\rangle^{1/2}(^{193}Po) = 0.22$ [15], coincides with that of the $^{184}Tl^{m3}$ ($I = 10$) and is thus preferable in the calculations. The resulting value of $\mu_{add}(\pi 1h_{9/2} \times \nu 1i_{13/2}) = 2.45(12)\mu_N$ agrees fairly well with the measured value: $\mu(10^-, ^{184}Tl) = 2.778(76)\mu_N$, thus supporting the proposed configuration assignment. It should be noted that similar considerations were applied to $^{186}Tl^m$ ($I = 10$) in Ref. [7].

Although the agreement between experimental and calculated values of $\mu(10^-, ^{184}Tl)$ is sufficient to confirm the leading configuration of the isomer in question, the examination of the isotopic trend of the magnetic moments for 10^- states shows that $\mu(10^-, ^{184}Tl)$ noticeably drops out of this trend (see Fig. 8 where the data for Tl isomers are compared with the data for Bi isomers with $I = 10$ [49,50]). Magnetic moments for the heavy odd-odd Bi isomers ($N = 119$–125) agree fairly well with the results of calculations by the additivity relation when μ_p from the magnetic moments of the adjacent odd-A Bi isotopes ($I = 9/2$) and μ_n from the magnetic moments of the adjacent odd-A Pb isomers ($I = 13/2$) are exploited. However, this approach does not work for the neutron-deficient ^{190,192,194}Bi ($N = 107, 109, 111$) isomers with $I = 10$. The agreement with the experiment may be restored by using $\mu_n = \mu(13/2^+, ^{195}Po) = -0.932\mu_N$ [15] (see Fig. 8). This choice is justified if one takes into account an increase in the mean-square deformation for the Bi isotopes and isomers at $N < 115$ [50] and the strong dependence of $\mu(\nu 1i_{13/2})$ on the deformation [15]. A reasonable agreement with the experiment for $^{186}Tl^m$ ($I = 10$) is achieved at $\mu_n = \mu(13/2^+, ^{193}Po) = -0.742\mu_N$ [15]. The aforementioned deviation of $\mu(10^-, ^{184}Tl)$ from the general trend of the magnetic moments of Bi and Tl 10^- isomers points to an increase in deformation of the 10^- state in ^{184}Tl compared to ^{186}Tl.

Magnetic moments for the 7^+ states in the chain of Tl isotopes are shown in Fig. 9. The rapid decrease in $\mu(\text{Tl}, I = 7)$ with the decrease in N at $A = 204$–198 has been explained by the assumption of the small admixture of $[\pi 1h_{11/2} \times \nu 3p_{3/2}]_{7+}$ and $[\pi 1h_{11/2} \times \nu 2f_{5/2}]_{7+}$ configurations to the leading $[\pi 3s_{1/2} \times \nu 1i_{13/2}]_{7+}$ configuration (Ref. [51], see also the discussion in Ref. [26]).

Indeed, magnetic moments for $^{186-196}$Tl are well described by the additivity relation for the $[\pi 3s_{1/2} \times \nu 1i_{13/2}]_{7+}$ configuration with μ_n and μ_p equal to the magnetic moments of the adjacent odd-A Tl and Hg isotopes (see Fig. 9). At the same time, magnetic moments for the configurations with the $1h_{11/2}$ proton are expected to be rather large: $\mu_{add}(\pi 1h_{11/2} \times \nu 3p_{3/2}; 7^+) = 5.42\mu_N$ and $\mu_{add}(\pi 1h_{11/2} \times \nu 2f_{5/2}; 7^+) = 6.14\mu_N$ (at $\mu_\nu(3p_{3/2}) = \mu(^{201}Hg) = -0.56\mu_N$, $\mu_n(2f_{5/2}) = \mu(^{203}Pb) = 0.69\mu_N$, and $\mu_p(1h_{11/2}) = \mu(^{197}Au) = 5.98\mu_N$ [49]). Correspondingly, a less than 10% admixture of these configurations is sufficient to describe the observed increase in $\mu(\text{Tl}, I = 7)$ from $0.5\mu_N$ to $1.2\mu_N$ when going from $A = 196$ to $A = 204$. Shell-model calculations by Kuo and Herling confirm the corresponding admixture of $(\pi 1h_{11/2})$-based configurations to the 7^+ state in ^{206}Tl (as cited in Ref. [51]). However, this explanation implies a rapid decrease in this admixture with the decrease in A and its disappearance at $A < 198$ to describe the observed μ trend. But such a disappearance seems to be contradicted by the known decrease in the excitation energy of the $1h_{11/2}$ proton-hole states in the adjacent odd-A Tl isotopes (see Fig. 9 in Ref. [3]). Further theoretical investigations are required in order to understand more quantitatively the nuclear structure of the 7^+ states in thallium isotopes.

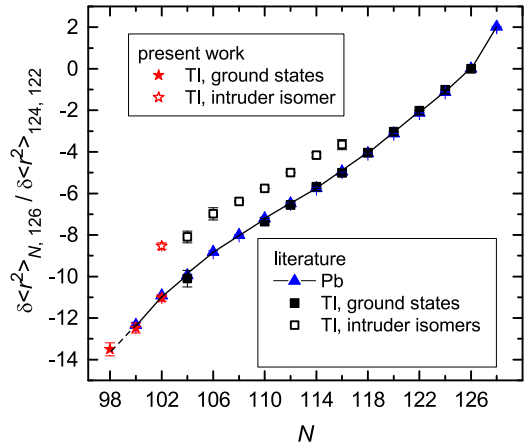

FIG. 10. Relative changes in $\delta\langle r^2\rangle$ for the even-neutron thallium and lead nuclei. Triangles: Pb [30,6]. Full squares: Tl (ground states) (Ref. [7] and references therein). Hollow squares: Tl (intruder isomers) (Ref. [7] and references therein). Full stars: Tl (ground states), present paper. Hollow star: Tl (intruder isomer), present paper.

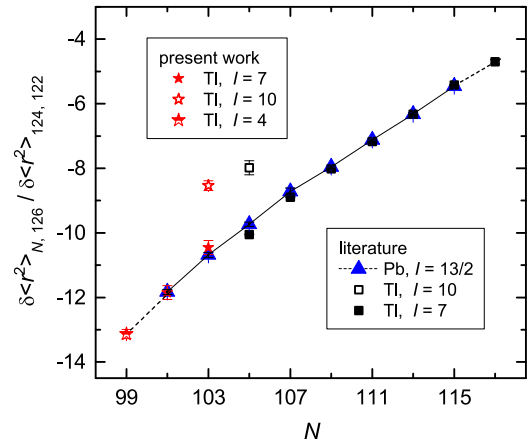

FIG. 11. Relative changes in $\delta\langle r^2\rangle$ for the odd-neutron thallium and lead nuclei. Triangles: Pb ($\nu 1i_{13/2}$ states) [30,6]. Full squares: Tl ($[\pi 3s_{1/2}, \nu 1i_{13/2}]_{7^+}$ states) (Ref. [7] and references therein). Hollow square: Tl (intruder isomer) [7]. Full stars: Tl ($[\pi 3s_{1/2}, \nu 1i_{13/2}]_{7^+}$ states), present paper. Hollow star: Tl (intruder isomer), present paper. Semihollow star: ^{180}Tl, present paper.

As seen in Fig. 9, the magnetic moment of ^{184}Tl drops out from the trend of the heavier Tl isotopes (and from the prediction of the additivity relation). This may be explained by the admixture of the $[\pi 2d_{3/2} \times \nu 1i_{13/2}]_{7^+}$ configuration: $\mu_{\rm add}(\pi 2d_{3/2} \times \nu 1i_{13/2}; 7^+) = -0.9\mu_N$ (at $\mu_n(1i_{13/2}) = \mu(^{185}{\rm Hg}) = -1.02\mu_N$ and $\mu_p(2d_{3/2}) = \mu(^{197}{\rm Au}) = 0.15\mu_N$ [49]). Thus, a 20% admixture of the $[\pi 2d_{3/2} \times \nu 1i_{13/2}]_{7^+}$ configuration is sufficient for decreasing $\mu(7^+, ^{184}{\rm Tl})$ from $0.6\mu_N$ (additivity relation prediction) to $0.4\mu_N$ (experimental value). It was found that in ^{184}Tl the retardation of the transition from the intruder-based (10^-) state to the (7^+) state is about seven times smaller than for the equivalent transition in ^{186}Tl [13]. This also hints towards the increased mixing of the $[\pi 2d_{3/2} \times \nu 1i_{13/2}]_{7^+}$ configuration in the (7^+) state of ^{184}Tl [13]. Definite conclusions about the corresponding mixing in $^{182}{\rm Tl}^{m2}$ cannot be made due to the large uncertainty of $\mu(7^+, ^{182}{\rm Tl}^{m2})$.

B. Changes in mean-square charge radii

In contrast to the mercury isotopic chain, where the strong odd-even staggering in the charge radii was found at $N < 106$ (see Ref. [4]), no such effect is observed for the ground states of the thallium isotopes (see Fig. 3). These states preserve their near-spherical shape beyond the neutron midshell ($A < 186$) and after the complete depletion of the $1i_{13/2}$ neutron shell ($A < 181$). The similar smooth behavior of $\delta\langle r^2\rangle$, testifying to the persistence of the near-spherical shape, was observed previously in the $^{182-208}$Pb isotopes ($N = 100$–126) [6].

To compare the different isotopic chains in the Pb region we use relative $\delta\langle r^2\rangle$: $\delta\langle r^2\rangle_{N,126}/\delta\langle r^2\rangle_{124,122} = \delta\nu^F_{N,126}/\delta\nu^F_{124,122}$ to avoid indeterminacy of the electronic factors. Figures 10 (even N) and 11 (odd N) show the relative changes in $\delta\langle r^2\rangle$ for the lead and thallium nuclei. For Pb nuclei the IS data from Refs. [30,6] were used. For the odd-N nuclei the data for states with the odd neutron in the same shell ($\nu 1i_{13/2}$) are displayed (the result for ^{180}Tl with a different neutron configuration is also shown for completeness). It clearly is seen that the Tl radii (both even N and odd N) perfectly follow the pattern of the Pb radii above and below the midshell at $N = 104$. Thus, the behavior of the thallium nuclei is clearly different from the lighter-Z elements Hg ($Z = 80$, Ref. [4]) and Au ($Z = 79$, Ref. [52]) in which a well-known pronounced deviation from sphericity has been observed.

Previously, a large isomer shift between the ground ($\pi 3s_{1/2}$) and the isomeric (intruder, $\pi 1h_{9/2}$) states in ^{185,191,193,195,197}Tl was found (see Ref. [7] and references therein). This shift was attributed to the increase in deformation for intruder isomers in comparison with the ground states. The same conclusion may be drawn for $^{183}{\rm Tl}^m$ studied in the present paper (see Figs. 3 and 10). Reference [53] includes calculations of deformations and excitation energies for the odd-mass thallium isotopes between $A = 181$ and 199 using the shell correction method with a Woods-Saxon potential and a monopole pairing residual interaction. These calculations predict that the difference in deformation (i.e., isomer shift) between the ground state and the isomeric state is nearly constant or even decreases below $A = 187$. However, an unexpected growth of the isomer shift (i.e., the mean-square deformation) relative to the heavier odd-A Tl nuclei was observed for ^{185}Tl [7] and ^{183}Tl (see Fig. 12). This growth was connected in Ref. [7] with the mixing and repulsion of two $9/2^-$ configurations. In ^{183}Tl with the $h_{9/2}$ proton intruder configuration two bands were associated with a strongly coupled spin sequence and a decoupled spin sequence which were interpreted as weakly deformed oblate and strongly deformed prolate structures [3,9]. The absolute value of the deformation of the prolate deformed $9/2^-$ state is expected to be markedly larger than that of the oblate deformed $9/2^-$ state [3,9]. If the band heads of these two configurations are in fact mixing, the mean-square deformation of the $9/2^-$ isomer would increase, compared to the moderate oblate deformation of the heavier thallium intruder isomers. Thus, the observed growth of the isomer shift when going

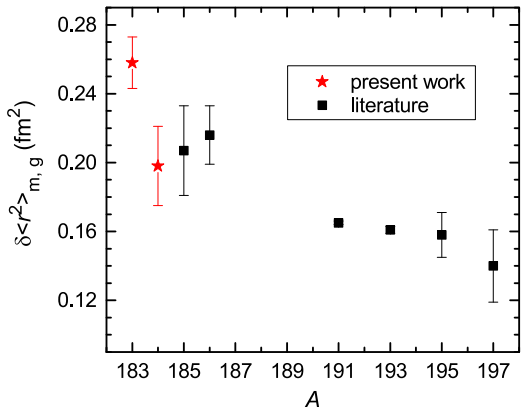

FIG. 12. Isomer shift between intruder and normal states for Tl isotopes. Stars: present paper. Squares: literature data (see Ref. [7] and references therein). Only statistical errors are shown.

from $A = 191$ to $A = 183$ may be explained by the increased mixing between the weakly deformed oblate and strongly deformed prolate structures.

For the first time the large isomer shift for the odd-odd Tl intruder isomer was found in ^{186}Tl [7]. A similar isomer shift for the 10^- isomer in ^{184}Tl was observed in the present paper (see Fig. 12). This finding supports the assumption of the same configuration $[\pi 1h_{9/2} \times \nu 1i_{13/2}]_{10^-}$ for the 10^--states in ^{186,184}Tl. The isomer shift in ^{186,184}Tl is similar to that of the adjacent odd-A Tl isotopes and may be interpreted in a similar way as the result of the increase in deformation in the corresponding isomers (see Fig. 3). This supports the shape-coexistence interpretation for these odd-odd isomers [2].

VI. CONCLUSIONS

Hyperfine structure parameters and isotope shifts have been measured for the neutron-deficient thallium isotopes ($A = 179$–184) using the 276.9-nm atomic transition. The measurements were performed at CERN-ISOLDE using the in-source resonance-ionization spectroscopy technique and Windmill setup for photoion current monitoring.

From the analysis of the hfs, spins for ^{179,181,183}Tl^g were determined to be $I = 1/2$. Magnetic moments and changes in the nuclear mean-square charge radii have also been deduced. A detailed analysis of the hyperfine structure patterns produced by different α and γ lines following the decay of ^{182}Tl confirms the existence of a low-spin isomer in ^{182}Tl. Magnetic moments of ^{179,181,183}Tl^g ($I = 1/2$) and ^{183}Tl^m [$I = (9/2)$] follow the respective parabolic and linear trends for the heavier Tl nuclei with the same spins. The application of the additivity relation for magnetic moments of the odd-odd Tl nuclei enables us to confirm leading configuration assignments and spins: $[\pi 3s_{1/2} \times \nu 1h_{9/2}]_{4^-}$ for ^{180}Tl and ^{182}Tl^{m1}; $[\pi 3s_{1/2} \times \nu 1i_{13/2}]_{7^+}$ for ^{182}Tl^{m2} and ^{184}Tl^{m2} (with the possible admixture of the $[\pi 2d_{3/2} \times \nu 1i_{13/2}]_{7^+}$ configuration); $[\pi 1h_{9/2} \times \nu 1i_{13/2}]_{10^-}$ for ^{184}Tl^{m3}.

The charge radii of the $^{179-184}$Tl ground states follow the trend previously observed for isotonic (spherical) lead nuclei. A significant difference in charge radii for ground and isomeric (intruder, $9/2^-$, and 10^-) states of ^{183,184}Tl is observed. The greater charge radii for the isomers suggest a larger deformation of these isomers compared to the ground states. The unexpected increase in the isomer shift for ^{183}Tl points to a possible prolate-oblate mixture.

ACKNOWLEDGMENTS

We would like to acknowledge the support of the ISOLDE Collaboration and technical teams. This work has been funded by FWO-Vlaanderen (Belgium), by GOA/2010/010 (BOF KU Leuven), by the Interuniversity Attraction Poles Programme initiated by the Belgian Science Policy Office (BriX network P7/12), by the European Commission within the Seventh Framework Programme through I3-ENSAR (Contract No. RII3-CT-2010-262010), by a grant from the European Research Council (Grant No. ERC-2011-AdG-291561-HELIOS), by a grant from the U.K. Science and Technology Facilities Council, by the Slovak Research and Development Agency under Contract No. APVV-15-0225, and by the Slovak grant agency VEGA (Contract No. 2/0121/14).

[1] K. Heyde, P. Van Isacker, M. Waroquier, J. L. Wood, and R. A. Meyer, Phys. Rep. **102**, 291 (1983).
[2] A. J. Kreiner, C. Baktash, G. Garcia Bermudez, and M. A. J. Mariscotti, Phys. Rev. Lett. **47**, 1709 (1981); M. Huyse, E. Coenen, K. Deneffe, P. Van Duppen, K. Heyde, and J. Van Maldeghem, Phys. Lett. B **201**, 293 (1988); P. Van Duppen, P. Dendooven, P. Decrock, M. Huyse, G. Reusen, and J. Wauters, Nucl. Phys. A **529**, 268 (1991).
[3] K. Heyde and J. L. Wood, Phys. Scr. **91**, 083008 (2016); Rev. Mod. Phys. **83**, 1467 (2011).
[4] G. Ulm *et al.*, Z. Phys. A: At. Nucl. **325**, 247 (1986).
[5] N. Bree *et al.*, Phys. Rev. Lett. **112**, 162701 (2014).
[6] H. De Witte *et al.*, Phys. Rev. Lett. **98**, 112502 (2007); M. D. Seliverstov *et al.*, Eur. Phys. J. A **41**, 315 (2009).
[7] A. E. Barzakh *et al.*, Phys. Rev. C **88**, 024315 (2013).
[8] W. Lauth *et al.*, Phys. Rev. Lett. **68**, 1675 (1992); J. A. Bounds *et al.*, Phys. Rev. C **36**, 2560 (1987); R. Menges *et al.*, Z. Phys. A: Hadrons Nucl. **341**, 475 (1992); H. A. Schuessler, E. C. Benck, F. Buchinger, and H. K. Carter, Nucl. Instrum. Methods Phys. Res., Sect. A **352**, 583 (1995).
[9] P. M. Raddon *et al.*, Phys. Rev. C **70**, 064308 (2004).
[10] A. N. Andreyev *et al.*, Eur. Phys. J. A **18**, 39 (2003).
[11] A. N. Andreyev *et al.*, Phys. Rev. Lett. **105**, 252502 (2010); Phys. Rev. C **87**, 054311 (2013); J. Elseviers *et al.*, *ibid.* **88**, 044321 (2013); V. Liberati *et al.*, *ibid.* **88**, 044322 (2013).
[12] J. Elseviers *et al.*, Phys. Rev. C **84**, 034307 (2011).
[13] C. Van Beveren *et al.*, Phys. Rev. C **92**, 014325 (2015).
[14] C. Van Beveren *et al.*, J. Phys. G Nucl. Part. Phys. **43**, 025102 (2016).
[15] M. D. Seliverstov *et al.*, Phys. Rev. C **89**, 034323 (2014).
[16] E. Kugler, Hyperfine Interact. **129**, 23 (2000).
[17] V. N. Fedosseev *et al.*, Rev. Sci. Instrum. **83**, 02A903 (2012).

[18] E. W. Otten, in *Treatise on Heavy-Ion Science*, edited by D. A. Bromley (Plenum, New York, 1989), Vol. 8, p. 517.
[19] G. Hermann, G. Lasnitschka, and D. Spengler, Z. Phys. D: At., Mol. Clusters **28**, 127 (1993).
[20] F. G. Kondev *et al.*, EPJ Web Conf. **63**, 01013 (2013).
[21] A. Lurio and A. G. Prodel, Phys. Rev. **101**, 79 (1956).
[22] http://www.nndc.bnl.gov/ensdf/
[23] J. E. Rosenthal and G. Breit, Phys. Rev. **41**, 459 (1932); A. Bohr and V. F. Weisskopf, *ibid.* **77**, 94 (1950).
[24] A. E. Barzakh *et al.*, Phys. Rev. C **86**, 014311 (2012).
[25] A.-M. Mårtensson-Pendrill, Phys. Rev. Lett. **74**, 2184 (1995).
[26] C. Ekström, G. Wannberg, and Y. S. Shishodia, Hyperfine Interact. **1**, 437 (1975).
[27] P. A. Moskowitz and M. Lombardi, Phys. Lett. B **46**, 334 (1973).
[28] J. R. Persson, Hyperfine Interact. **162**, 139 (2005).
[29] G. Torbohm, B. Fricke, and A. Rosén, Phys. Rev. A **31**, 2038 (1985).
[30] G. Fricke and K. Heilig, *Nuclear Charge Radii* (Springer, Berlin, 2004).
[31] A. C. Hartley and A.-M. Mårtensson-Pendrill, J. Phys. B: At. Mol. Opt. Phys. **24**, 1193 (1991); A. C. Hartley, A.-M. Mårtensson-Pendrill, and A. Ynnerman (private communication cited in Ref. [6]).
[32] D. Berdichevsky and F. Tondeur, Z. Phys. A: At. Nucl. **322**, 141 (1985).
[33] B. Pritychenko, M. Birch, B. Singh, and M. Horoi, At. Data Nucl. Data Tables **107**, 1 (2016).
[34] R. Neugart *et al.*, Phys. Rev. Lett. **55**, 1559 (1985).
[35] A. Arima and H. Sagawa, Phys. Lett. B **173**, 351 (1986).
[36] P. Rahkila *et al.*, Phys. Rev. C **82**, 011303 (2010).
[37] A. N. Andreyev *et al.*, Phys. Rev. C **80**, 024302 (2009).
[38] M. P. Carpenter, F. G. Kondev, and R. V. F. Janssens, J. Phys. G Nucl. Part. Phys. **31**, S1599 (2005).
[39] A. N. Andreyev *et al.*, Phys. Rev. C **80**, 054322 (2009).
[40] A. Melerangi *et al.*, Phys. Rev. C **68**, 041301(R) (2003).
[41] D. O'Donnell *et al.*, Phys. Rev. C **79**, 051304(R) (2009).
[42] B. Marsh *et al.* (unpublished).
[43] S. Nagamiya and T. Yamazaki, Phys. Rev. C **4**, 1961 (1971).
[44] H. Hübel, Fortschr. Phys. **26**, 327 (1977).
[45] A. Bouljedri *et al.*, Z. Phys. A: Hadrons Nucl. **339**, 311 (1991).
[46] A. N. Andreyev *et al.*, Eur. Phys. J. A **18**, 55 (2003).
[47] E. Rapisarda *et al.* (unpublished).
[48] J. D. Cole *et al.*, Phys. Rev. Lett. **37**, 1185 (1976).
[49] N. J. Stone, At. Data Nucl. Data Tables. **90**, 75 (2005).
[50] A. E. Barzakh *et al.* (unpublished).
[51] O. Hashimoto *et al.*, Nucl. Phys. A **218**, 180 (1974).
[52] K. Wallmeroth *et al.*, Nucl. Phys. A **493**, 224 (1989).
[53] G. J. Lane *et al.*, Nucl. Phys. A **586**, 316 (1995).